

Experimental and finite element parametric investigations of the thermal behavior of CBGB

Hesham A. Numan^{*}, Nildim Tayşı^a and Mustafa Özakça^b

Department of Civil Engineering, University of Gaziantep, 27310, Gaziantep, Turkey

(Received November 23, 2015, Revised December 02, 2015, Accepted December 11, 2015)

Abstract. This research deals with the behavior of Composite Box Girder Bridges (CBGBs) subjected to environmental effects such as solar radiation, atmospheric temperature, and wind speed. It is based on temperature and thermal stress results, which were recorded hourly from a full-scale experimental CBGB segment and Finite Element (FE) thermal analysis. The Hemi-cube method was adopted to achieve the accuracy in temperature distributions and variations in a composition system during the daily environmental variations. Analytical findings were compared with the experimental measurements, and a good agreement was found. On the other hand, parametric investigations are carried out to investigate the effect of the cross-section geometry and orientation of the longitudinal axis of CBGB on the thermal response and stress distributions. Based upon individual parametric investigations, some remarks related to the thermal loading parameters were submitted. Additionally, some observations about the CBGB configurations were identified, which must be taken into account in the design process. Finally, this research indicates that the design temperature distribution with a uniform differential between the concrete slab and the steel girder is inappropriate for describing the thermal impacts in design objective.

Keywords: composite box girder bridge; environmental effects; temperature distribution; parametric thermal investigation

1. Introduction

Because of the advances in steel construction technology, the use of steel trapezoidal box girders in urban highway has become extensive. The higher flexural capacity, higher torsion stiffness, rapid erection, economics, long span capability, and aesthetics of these girders make them more convenient compared to other structural systems (Topkaya *et al.* 2005).

The behaviors of CBGBs are distinctly affected by the surrounding climatic actions due to these structures are erected in open environments. The surrounding climatic actions involve basically: solar radiation intensity, atmospheric temperature, and wind speed, which are all fluctuating with time. These changes of climatic actions are generally caused complex temperature changes that vary in intensity and distribution within the bridge throughout the day and the year.

Generally, regardless of whether the cross-section of CBGB is unrestrained at the supports or

^{*}Corresponding author, Lecturer, E-mail: heshamnuman@yahoo.com

^aAssistant Professor, E-mail: taysi@gantep.edu.tr

^bProfessor, E-mail: ozakca@gantep.edu.tr

not, the nonlinear sectional temperature distribution will induce eigenstresses (self-equilibrating stresses). Based upon the Bernoulli-Euler hypothesis that plane sections remain plane after deformation, the eigen thermal stresses develop over the cross-section of bridge to strain the fibers to lie in one plane. The resulted stresses cause to further deformation in the bridge girder section and this may lead to formation of temperature cracks in the concrete slab.

The early field measurements were conducted in composite steel bridges which undergoing environmental thermal effects to show temperature distribution along the depth of superstructures and tried to predict formulas of the maximum temperature gradients performed by (Naruoka *et al.* 1957), Barber (1957), Zuk (1965), Berwanger (1970), and Berwanger and Symko (1975). Im and Chang (2004) also carried out a field study on a composite box-girder viaduct, which was located in the south of Seoul, from April 1997 to April 1998 to estimate the thermal loading parameters. The authors were confirmed that the transverse temperature differences in CBGB are no longer negligible due to their similarity in magnitude as those for vertical temperature differences, especially in the winter months of the year.

The temperature distribution over the depth of CBGB under environmental thermal loadings was studied by developing a computer program based on a finite difference formulation with arbitrary geometry and orientation for a given geographic location and environmental factors submitted by (Dilger *et al.* 1983).

The extreme effective temperatures of concrete deck in the steel-concrete bridge in Hong Kong were investigated based on the theory of extreme value analysis with a certain return period accomplished by Ni (Ni *et al.* 2007). Xu (Xu *et al.* 2010) revealed that the ambient air temperature has similar variation patterns to those of the effective bridge deck temperature based upon the measured data from 1997 to 2005 on the Tsing Ma Bridge.

Cao (Cao *et al.* 2011) observed that the maximum temperature gradient in the steel section was more than twice the design specification; also they found that the concrete temperature lagged obviously behind surrounding air about five to six hours, while cable temperatures stayed between those of concrete and surrounding air. These observations were recorded according to the structural health monitoring system on the Zhanjiang Bay Bridge.

The climatic conditions may earnestly affect on the design life of the bridges by causing cracks in the concrete deck or deflections emphasized by Stewart (1967), Kennedy and Soliman (1987), Massicotte (Massicotte *et al.* 1994), and William (William *et al.* 2005).

On the other hand, the numerical studies were carried out by Berwanger (1983), Fu (Fu *et al.* 1990), Tong (Tong *et al.* 2001), Kim (Kim *et al.* 2009), Larsson and Karoumi (2011), and Xia (Xia *et al.* 2013) by using two-dimensional (2D) and three-dimensional (3D) FE models to investigate the state of heat flow and temperature profiles of composite bridge structures under environmental thermal conditions. In addition, Emanuel and Hulsey (1978) employed FE model to determine the vertical temperature distribution over the cross-section of a composite bridge by considering concrete as an isotropic and homogeneous. The authors found that the climatic conditions had the primary effect on the temperature distribution through the section of composition system.

Both of displacement and restraint force occurring at the bridge bearings under summer and winter thermal loading for a composite steel highway viaduct were predicted by utilizing 3D FE with MSC/NASTRAN software by Troy and Chai (1998).

The influences of change in environmental temperature on the mode shape curvatures and frequencies of a cable-stayed bridge were studied by using FE simulation performed by Xu and Wu (2007). Moorty and Roeder (1992) and Chang and Robertson (2003) employed the FE program ANSYS to simulate both of the thermal movements and the deformations for concrete-

steel composite girders.

The main objective of the present paper is to simulate and assess the influences of geometrical parameters and orientation of the bridge’s longitudinal axis on the thermal behavior of CBGB. To fulfill this objective, an experimental, full-scale CBGB segment was constructed in Gaziantep City, and FE studies were carried out and will be briefly presented in this work. The most important of parametric investigations needed to analyze the influence of cross-section geometry and orientation of the bridge’s longitudinal axis on the thermal response and stress distributions in CBGB are conducted. The realistic ranges for each parametric investigation could be used to develop the visibility of the fundamental thermal response of such constructions.

The current study also is focused on improving the understanding of FE heat transfer analysis of CBGB through emulating mutual irradiations between the exposed bridge surfaces and the ambient air concurrently. Besides to the transient heat conduction, surface convection, solar radiation, and reflected radiation were modeled. All these considerations are considered as the most important effects that must be taken into account in thermal analysis for such structures to achieve the accuracy of the temperature field within portions.

After carrying out a comprehensive search, to the best of the authors’ knowledge besides the literature survey of this research, none of the previously reviewed works contained reciprocal irradiations between the external surfaces of CBGB along the daily thermal cycle.

2. Heat transfer analysis of composite bridges

The heat conduction process within a composite bridge can be simulated through the Fourier partial differential equation, which is expressed as follows

$$k \left(\frac{\partial^2 T}{\partial x^2} + \frac{\partial^2 T}{\partial y^2} + \frac{\partial^2 T}{\partial z^2} \right) + Q = \rho c \frac{\partial T}{\partial t} \quad (1)$$

where k is the isotropic thermal conductivity coefficient of the material in W/mK; T is the temperature at an arbitrary point (x , y , and z) in K; Q is the rate of heat generated per unit volume of concrete material in W/m³; ρ is the density of the material in kg/m³; c is the specific heat of the material in J/kgK; and t is the time. The boundary conditions associated with Eq. (1), can be expressed as follows

$$k \left(\frac{\partial T}{\partial x} l_x + \frac{\partial T}{\partial y} l_y + \frac{\partial T}{\partial z} l_z \right) + q = 0 \quad (2)$$

where l_x , l_y , and l_z are the direction cosines of the unit outwards vectors normal to the boundary surfaces of the bridge; and q is the sum of all heat fluxes occurs on the bridge surfaces in W/m², which can be expressed as

$$q = q_{co} + q_{sr} + q_{re} + q_{ir} \quad (3)$$

The term q_{co} denotes the convection heat transfer that happens between the surrounding air and the bridge surfaces because of the temperature difference between them, and can be described as

$$q_{co} = h_{co} (T_s - T_a) \quad (4)$$

where h_{co} is the convection coefficient between the surrounding air and the bridge surfaces in W/m^2K ; T_s is the surface temperature of the bridge in K ; and T_a is the temperature of surrounding air in K . In the present study, the used following empirical formulas were originally recommended by Kehlbeck (1975) to assess the convection coefficients h_{co} for CBGB

$$h_{co} = 3.83\omega + 4.67 \quad (5)$$

$$h_{co} = 3.83\omega + 2.17 \quad (6)$$

$$h_{co} = 3.83\omega + 3.67 \quad (7)$$

$$h_{co} = 3.5 \quad (8)$$

Eqs. (5)-(8) were utilized to compute the convection on the top surface of the bridge, the bottom surfaces of the bridge, the webs of the external surfaces of the bridge, and the indoor surfaces of the box girder, respectively. The term ω refers to the wind velocity in m/s .

q_{sr} is the incoming heat fluxes from global solar radiation on the exterior boundary surfaces of the bridge, which is represented by

$$q_{sr} = \alpha_t I_{sr} \quad (9)$$

where α_t is the absorption coefficient of the bridge surfaces; and I_{sr} is the global solar radiation received by horizontal surface of the bridge in W/m^2 .

q_{re} is the reflected radiation from the ground surface and from other objects surrounding the bridge in W/m^2 that is also defined as albedo and can be calculated as

$$q_{re} = \alpha_t I_{re} \quad (10)$$

$$I_{re} = r_g I_{sr} \frac{1 - \cos \delta}{2} \quad (11)$$

where I_{re} is the reflected radiation flux from the ground and the surroundings in W/m^2 ; r_g is the reflection coefficient of the ground and from other objects surrounding the bridge; and δ is the inclination angle of the surfaces of bridge respect to the horizontal.

q_{ir} is the irradiation heat transfer between the exposed bridge surfaces and ambient air can be expressed using Stefan– Boltzmann law

$$q_{ir} = \varepsilon S (T_s^4 - T_a^4) \quad (12)$$

where ε is the emissivity coefficient of bridge surface; and S is the Stefan-Boltzman constant, which equals to $5.67 \times 10^{-8} W/m^2K^4$.

3. Experimental analysis of CBGB segment

In this research, experimental work, using the full-scale, CBGB segment that is illustrated in Fig. 1, was conducted on the campus of Gaziantep University, Turkey at Latitude: 37° 02' 22" N

and Longitude $37^{\circ} 19' 07''$ E and the longitudinal axis of the bridge segment is located on the East-West direction. The purpose of the experimental work was to study both of the temperature distributions and thermal stresses in CBGB under the environmental thermal loads. Fig. 2 shows the cross-section details of the experimental CBGB segment, while the length of the bridge segment is 2.0 m. The internal braces and stiffener plates were held inside the steel section at the middle span to increase both of the stabilization and the torsional stiffness of the composite structure.

The bridge segment was erected on four reinforced concrete columns, as illustrated in Fig. 1. These columns were constructed to lift the CBGB above the ground surface to emulate the realistic ground reflected radiation and to permit free fluent of air to the lower surface of the bottom flange of the steel girder to emulate realistic convection cooling. For the deck portion and the supporting columns, normal concrete was used and the standard steel alloy ASTM A36 was employed for all parts of the girder.

Three layers of plywood were placed at the contact surfaces between the supporting columns and CBGB segment to abolish the role of supporting columns in the heat transfer process of CBGB.

After the expiry of the curing period for the concrete slab, the faces of the cross-section of CBGB were covered by special insulation boards to assure the thermal isolation along the cavity of the bridge, as illustrated in Fig. 1. This insulation is significant to analyze the actual status in most CBGBs, where no sunlight or air fluxes inside the cavity of the bridge.

Sensors, involving thermocouples type-T, Vibrating Wire (VW) strain gauges, 108-temperature probe, CS3 pyranometer and NRG#40 anemometer were used to measure temperatures of both the concrete slab and steel girder, thermal stress for each component of CBGB, air shade temperature, global solar radiation and wind speed, respectively. The data acquisition system was included mainly: CR1000 data logger, three AM16/32 multiplexers, and AVW200 spectrum analyzer. The data logger was programmed to read and storage the experimental records at one hour intervals.

As shown in Fig. 3(a), thirty-two thermocouples were installed in the mid-span section of CBGB segment and were divided into eight sets (A, B, C, D, E, F, G, and H). Set (A, E, and G)

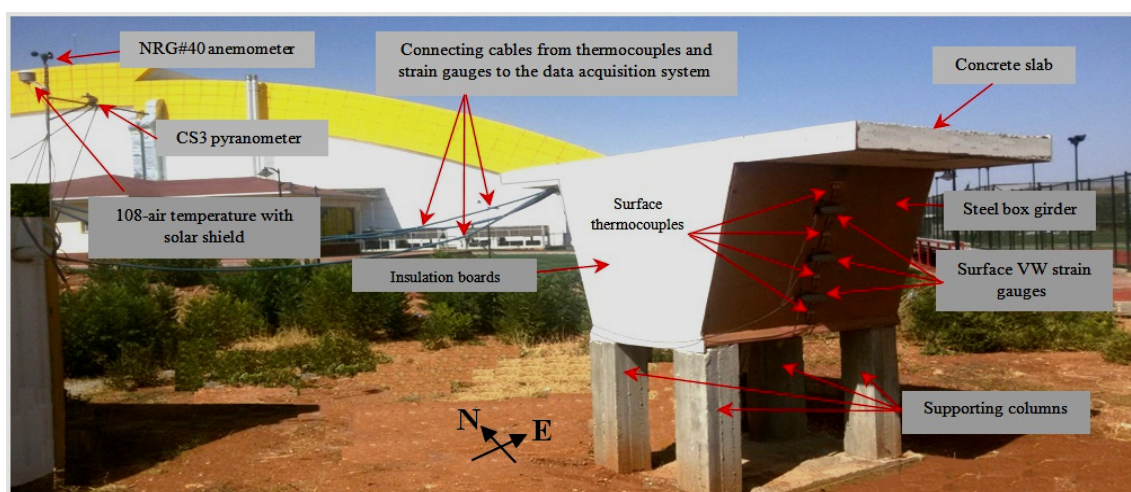


Fig. 1 The experimental CBGB segment

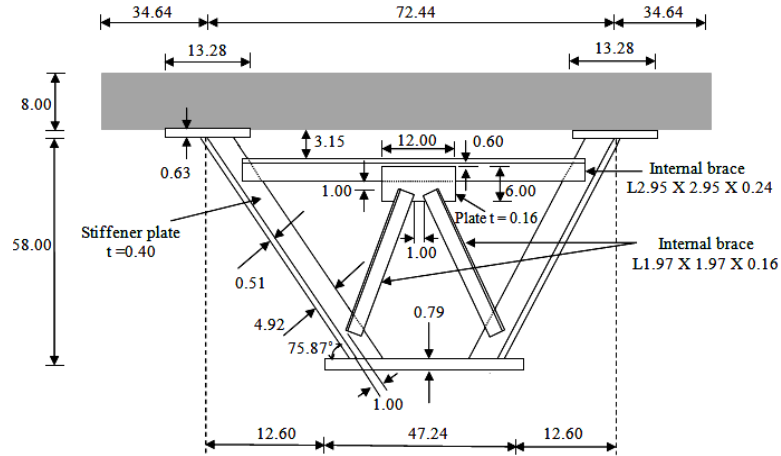


Fig. 2 Cross-section of the experimental CBGB segment (all dimensions in inches and not to scale)

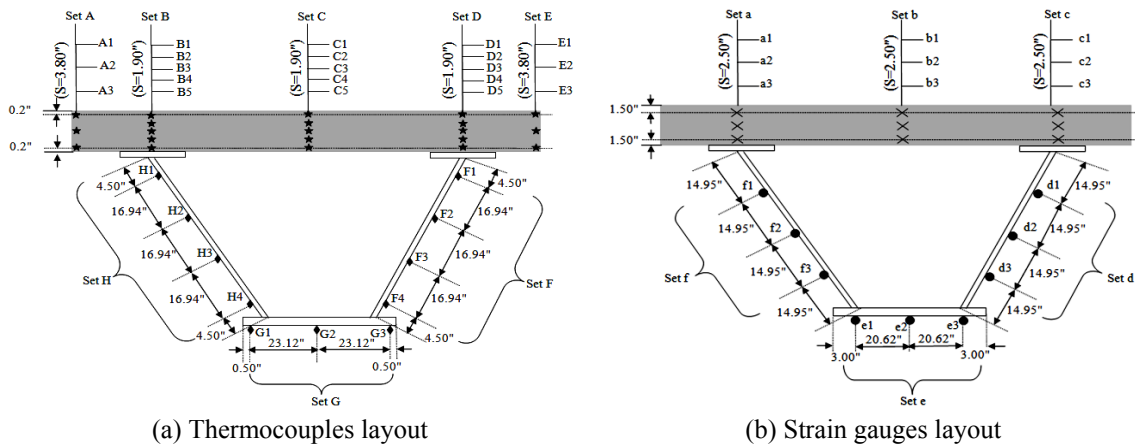


Fig. 3 Thermocouples and strain gauges layouts within the experimental CBGB segment

consists of three thermocouples and each of the sets (F and H) has four thermocouples, while the remaining set (B, C, and D) has five thermocouples each.

Fig. 3(b) depicts the distribution of thirteen strain gauges, which is also in the mid-span section of CBGB segment and divided into six sets (a, b, c, d, e, and f). Each set has three VW strain gauges. In Fig. 3, the character *S* refers to the spacing between thermocouples and strain gauges inside the concrete slab from center to center.

It should be noted that the surface VW strain gauges and the surface of thermocouples are covered with special plastic lids to protect both of them from the external factors (e.g., from water on a rainy day and direct sun rays, etc.) that may affect the readings.

4. FE thermal analysis of CBGB

CBGB model was constructed based on FE simulation by using a commercial program

COMSOL to simulate the environmental thermal impacts on the bridge.

Exchanging (reciprocal) irradiations flux at the exterior surface of the bridge that arising from both ambient air and other surfaces were simulated by using the surface-to-surface radiation interface, which is the most complicated part of the current 3D thermal analysis. This complexity happens due to the use of surface-to-surface radiation interface under Hemi-cube method that accounts the shadow effect on the external faces of the bridge at each time step. The effect of shadowing on bridge body will be calculated through orienting the digital camera in five different directions to identify the view factor. However, the irradiative heat flux at the exposed surface of the bridge was modeled by the following expression

$$q_{ir} = \varepsilon(G_{ir} + F_a ST_s^4 - ST_a^4) \tag{13}$$

where G_{ir} is the reciprocal irradiation arriving from other surfaces in W/m^2 (is a function of the radiosity at any other point in view); and F_a is the ambient view factor, i.e. prescribes the fraction of view from each point that is not covered by other boundaries. To reduce the time of analysis and to speed up the radiosity simulation, the external surfaces of the experimental CBGB segment were assembled into four sets (north, south, upper, and lower), where each set included one surface or more which depends on the location of surface in bridge segment. Therefore, the radiation group feature was activated. It should be noted that the process of assembling surfaces has been done with maintaining the differences in surface emissivity and surface absorptivity for each material.

Thermal material properties used to build the present CBGB model are given in Table 1. These properties were assumed to be isotropic and independent of time. Moreover, the albedo was taken as 0.25.

To simplify the problem of the thermal performance of the composition system, the difference between coefficients of thermal expansion of concrete and steel was ignored and the mean value was considered, as 6.25×10^{-10} in/in/°F, in addition to, the Bernoulli-Euler hypothesis that the plane sections remain plane after deformation was valid.

The temperature distribution along the longitudinal axis of the bridge is assumed to be constant since the CBGB segment is straight and with uniform cross-sections along the bridge's length. Therefore, only one cross-section in the mid-span of bridge was taken into account to simulate the thermal loading parameters. These thermal loading parameters can be defined as follows: T_v is the vertical linear temperature difference; T_h is the horizontal linear temperature difference; T_m is the mean bridge temperature; and T_{res} is the residual temperature which contributes to produce eigenstresses within the cross-section of CBGB model. The following formulas are the thermal loading parameters that used in the FE parametric investigations.

Table 1 Values of the thermal material properties

Material properties	Concrete	Steel
Thermal conductivity (W/mK), k	1.50	46
Specific heat (J/kgK), c	950	486
Absorptivity, α	0.65	0.88
Emissivity, ε	0.80	0.60
Density (kg/m^3), ρ	2400	7850

$$T_v = H \frac{\int_{A_c} E_c T(x, y, t) y dA + \int_{A_s} E_s T(x, y, t) y dA}{\int_{A_c} E_c y^2 dA + \int_{A_s} E_s y^2 dA} = \frac{\sum_{i=1}^k E_k T_k A_k y_k}{\sum_{i=1}^k E_k A_k y_k^2} \quad (14)$$

$$T_h = W \frac{\int_{A_c} E_c T(x, y, t) x dA + \int_{A_s} E_s T(x, y, t) x dA}{\int_{A_c} E_c x^2 dA + \int_{A_s} E_s x^2 dA} = \frac{\sum_{i=1}^k E_k T_k A_k x_k}{\sum_{i=1}^k E_k A_k x_k^2} \quad (15)$$

$$T_m = \frac{\int_{A_c} E_c T(x, y, t) dA + \int_{A_s} E_s T(x, y, t) dA}{\int_{A_c} E_c dA + \int_{A_s} E_s dA} = \frac{\sum_{i=1}^k E_k T_k A_k}{\sum_{i=1}^k E_k A_k} \quad (16)$$

where E is the modulus of elasticity; A is the area of the cross-section; x and y are Cartesian coordinates; $T(x, y, t)$ is the temperature field change at each time step of analysis; the subscript c , s , and i refer to the concrete material, the steel material, and the index of the node in the cross-section, respectively; H and W are the depth and width of the cross-section, respectively.

At a certain time, the residual temperature can be evaluated by subtracting the linear components from the temperature field change as given in the following form

$$T_{res} = T(x, y, t) - \frac{\Delta T_v}{H} y - \frac{\Delta T_h}{W} x - T_m \quad (17)$$

Due to thirty-two thermocouples are distributed in different locations of the experimental CBGB segment. Therefore, it is appropriate to impose the initial bridge temperature to be equal to the mean temperature of these thermocouples better than atmospheric temperature. In this study, the initial bridge temperature was taken at 04:00 a.m., when the temperature distribution is generally close to uniform at this time. To diminish the influence of imposing the initial bridge temperature on the thermal response of the bridge in our work, we included the combined environmental thermal loading of solar radiation, atmospheric temperature and wind speed before three days from the intended day.

As a result of identifying the location of the bridge, time zone, date, time, and maximum solar irradiance, the solar radiation model in COMSOL will compute automatically the direction and intensity of the sun's incident radiation on CBGB at each time step throughout the day.

5. Comparison of experimental and analytical results

In order to validate temperatures and thermal stresses of the FE analysis results, the calculated values were compared with those gathered from experimental measurements of CBGB segment. The comparisons were done in an arbitrary clear day from the summer season for Gaziantep,

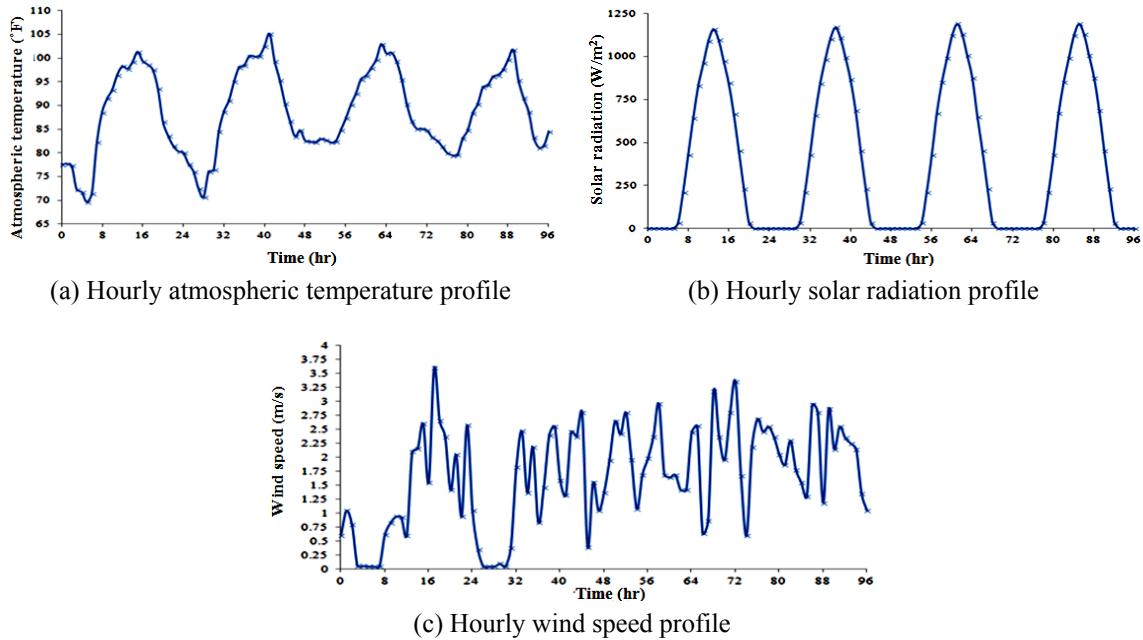


Fig. 4 Climatic conditions for August 3

Turkey, which was August 3, 2015, and especially after the heat wave that engulfed the whole Turkey in this season. Since the ambient air temperatures around Turkey have been increased from 5-9°C above the seasonal averages based on the Turkish State Meteorological Service. Therefore, this heat wave was an opportunity to give a better visualization on the trend of thermal loading parameters, and hence, it contributes to supplement the thermal actions provisions for CBGB design in Turkey. The hourly climatic measurements involving atmospheric temperature, global solar radiation and wind speed on August 3 were used as the thermal load inputs of the FE model and shown in Fig. 4.

Two statistical measurements were carried out to investigate the degree of agreement between the experimental and the analytical temperature results. The first one was the Maximum Absolute Error (MAE), and it refers to the maximum absolute difference between the experimental and the analytical temperatures at each thermocouple site during the analyzed day. The second measurement was the Average Absolute Error (AAE) that is the summation of the absolute differences between the analytical and the experimental temperatures at each thermocouple site divided by the total number of time steps of the analyzed day. Smaller values of MAE and AAE signify that the degree of agreement between the experimental and the analytical temperature results is good.

Fig. 5 illustrates the comparisons between the experimental and the analytical temperatures on August 3, 2015 for arbitrary thermocouples (C1, C3, C5, F3, H3, and G2). These thermocouples were selected to be the representative temperatures across the vertical symmetry axis for the concrete slab, as well as, for the south, north and lower webs of steel girder. In this figure, EXP indicates to experimental results, while ANA indicates to the presented analytical 3D model results. The MAE was within the range of 2.66 to 3.30°F, while the AAE was within the range 0.50 to 1.45°F for chosen thermocouples. Thus, the variations and the magnitudes of the analytical

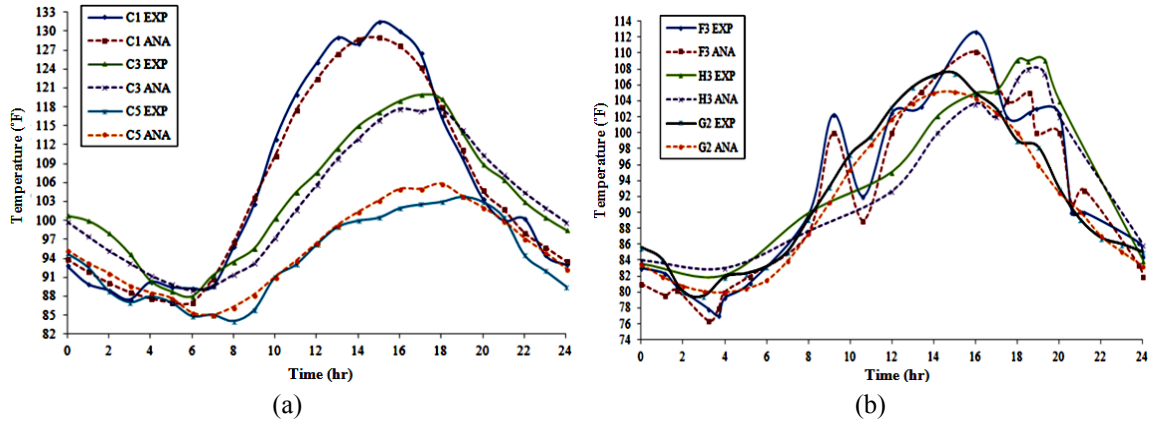


Fig. 5 Comparison of experimental and analytical temperatures on August 3: (a) thermocouples C1,C3, and C5; (b) Thermocouples F3, H3, and G2

temperatures matched well with the experimental ones. The range of MAE and AAE for all sets of thermocouples was listed in Table 2.

From Fig. 5(a), thermocouple C1 has the highest value of experimental and analytical temperatures than those thermocouples C3 and C5. This can be attributed to the top horizontal concrete surface of the bridge was subjected to the direct beam radiation for long hours during the daytime and thus this surface becomes hotter than the interior layers and the bottom surface.

From obvious results in Fig. 5(b), the peak value of experimental and analytical temperatures take place at thermocouple F3. This is owing to the southern faces of steel girder what received more incident solar radiation than the other faces as a result of the sun movement during the summer’s day.

From Table 2, the largest temperature error of MAE for a CBGB section was 4.70°F. On the other hand, the maximum temperature error of AAE in the concrete slab and steel girder was 1.80°F and 1.60°F, respectively. Hence, the values of MAE and AAE in Table 2 proved that the experimental temperatures were very close to the analytical temperatures for the proposed sites of thermocouples during 24 hours of chosen day.

The comparison between experimental and analytical longitudinal eigenstress distributions at 01:30 p.m. and 05:00 a.m. were also utilized as another validation tool, as illustrated in Fig. 6. In

Table 2 MAE and AAE of the experimental and the analytical temperatures on August 3 during the 24 hours period

Statistical measurement		Section			
		Concrete slab		Steel girder	
	Range	Value (°F)	Site of thermocouple	Value (°F)	Site of thermocouple
MAE	Min.	1.40	B3	2.20	F2
	Max.	4.70	D5	2.80	H1
AAE	Min.	0.50	C1	1.00	H3
	Max.	1.80	A2	1.60	G3

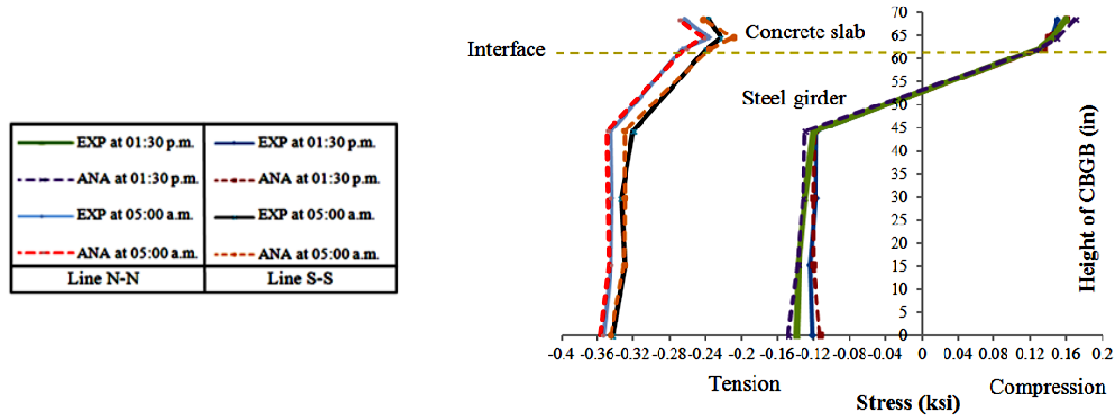


Fig. 6 Longitudinal eigenstress distributions along the southern and northern sides of bridge at time of maximum compressive and tensile stresses for the concrete slab

this figure, Line S-S refers to the line that passes through the VW strain gauges on the southern side of the bridge, while Line N-N refers to the line that passes through the VW strain gauges on the northern side of the bridge.

At 01:30 p.m., the longitudinal stress distributions of concrete slab behave as compressive, while the longitudinal stress distributions of the steel girder were tensile for the proposed two lines. This is due to the incident solar radiation on the concrete slab and the entirely shaded steel girder at this time. At 05:00 a.m., the absence of solar radiation and low atmospheric temperature were worked to reverse the longitudinal stress distributions of the concrete slab from compressive to tensile and an increase of the tensile values of the steel girder as compared with readings of the two lines in the previous case.

From Fig. 6, it may be observed that the significant differences between the experimental and the analytical longitudinal stress distributions result (Line S-S and Line N-N) do not exist.

Therefore, these realities and agreement of the results gives us a good indicator that the present FE analysis is efficient.

6. Parametric investigations

To characterize the behavior and trend of the thermal loading parameters during the daily thermal cycle on CBGB, four parametric investigations involving: orientation of the bridge’s longitudinal axis, cantilever length of the concrete slab, depth of steel girder and thickness of concrete slab are implemented. The thermal loading parameters were vertical and horizontal linear temperature difference, mean bridge temperature, and average residual temperature in the concrete slab and steel girder, respectively. When studying the effect of a chosen parameter, the other parameters were kept constant. The solar radiation, atmospheric temperature, wind speed and albedo of August 3 were used as the inputs of the environmental thermal loads. Table 3 lists the details of the four parametric investigations.

Although 14 inches thickness is seldom used in design practice of composite steel girders, it was included to investigate the trend of temperature variation over the section. The results of the thermal loading parameters under the parametric investigations will be graphed and discussed

Table 3 Details of the four parametric investigations

Study	Parameter	Variation range	Variation step
1	Bridge orientation (β) [*] (deg.)	0-90	30
2	Cantilever length of concrete slab (L) (in.)	28-82	18
3	Depth of steel girder (H) (in.)	58-124	22
4	Thickness of concrete slab (T) (in.)	8-14	2

^{*} β : is the angle between the longitudinal axis of CBGB and towards the north direction

briefly in the following subsections:

6.1 The vertical linear temperature difference

From Fig. 7(a), it can be noted that from 05:40 a.m. (at the onset of the sunrise) to around 11:00 a.m., the vertical linear temperature difference began to gradually decrease when the orientation of bridge turned from $\beta = 0^\circ$ to $\beta = 90^\circ$ until reaching the highest negative value at $\beta = 90^\circ$ at about 09:30 a.m. In addition, the vertical linear temperature difference became lower at $\beta = 90^\circ$ compared to the other orientations beyond 03:30 p.m. to about 08:00 p.m. These cases can be explained due to receiving more sunlight by the northern and southern faces of steel girder at $\beta = 90^\circ$ than the other three orientations and as a result the steel girder was heated up faster.

Longer cantilever lengths led to the largest shaded area on the steel faces than the other cantilever lengths and their temperature decreased faster. Therefore, increasing the cantilever length of concrete slab from 28 to 82 inches resulted in an increase the vertical linear temperature difference from around 07:30 a.m. to around 11:00 a.m., as well as, for the period from about 03:30 p.m. to about 07:00 p.m., as shown in Fig. 7(b).

From Fig. 7(c), it is clearly observed that the variances between gradients substantially achieved at times when the faces of steel girder were subjected to direct sunshine. Otherwise, the variances between gradients at other times of the examined day were quite small. The vertical thermal gradient decreased at a higher rate from the shortest to the longest steel web depth from about 07:00 a.m. to about 11:50 a.m. In contrast, the vertical thermal gradient became higher in the section of CBGB with the shortest steel web depth compared to other depths at the period from about 12:05 p.m. to about 05:40 a.m. This is due to the shortest steel web depth in both of northern and southern side of the bridge worked to minimize the ratio of sunlit area in steel webs than those for other depths and thus their temperature were lost quicker.

From Figs. 7(a)-(c), the peak positive of the vertical linear temperature difference occurred at about 08:30 p.m., and it seemed to be independent of the orientation of the longitudinal axis of the bridge, the cantilever length of the concrete slab, and the depth of the steel girder. This is because the steel girder lost most of its heat after a short time of the sunset, while the concrete slab stilled keeping some of the heat from the daylight hours of the examined day.

The increment of concrete slab thickness was accompanied by an increase in the internal layers within it. This causes that the thickest concrete slab retained of heat for a relatively long time more than the other thicknesses, as a result, the heat flux between the internal layers of concrete by conduction is very slow. Therefore, the gradient climbed during the dark hours to about 11:00 a.m. and dropped after 11:00 a.m. to about 08:30 p.m.; and the maximum vertical linear temperature difference occurred at 12:00 a.m. at the section with the thicker concrete slab, as shown in Fig. 7(d).

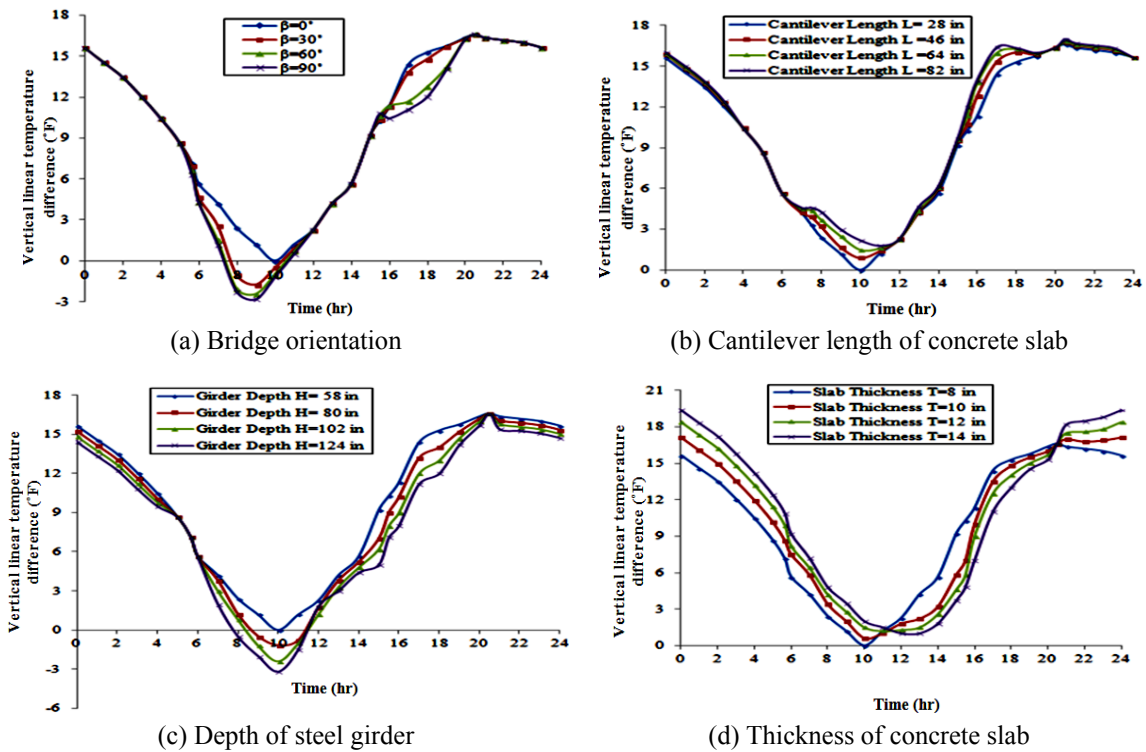


Fig. 7 Parametric investigations of the vertical linear temperature difference

6.2 The horizontal linear temperature difference

From Fig. 8(a), it is clearly can be shown that the orientation of the longitudinal axis of CBGB has a significant effect on the horizontal linear temperature difference. When the longitudinal axis of bridge settled at $\beta = 90^\circ$, the predicted maximum positive and negative horizontal linear temperature differences were recorded at around 07:30 a.m. and 07:00 p.m., respectively. This is

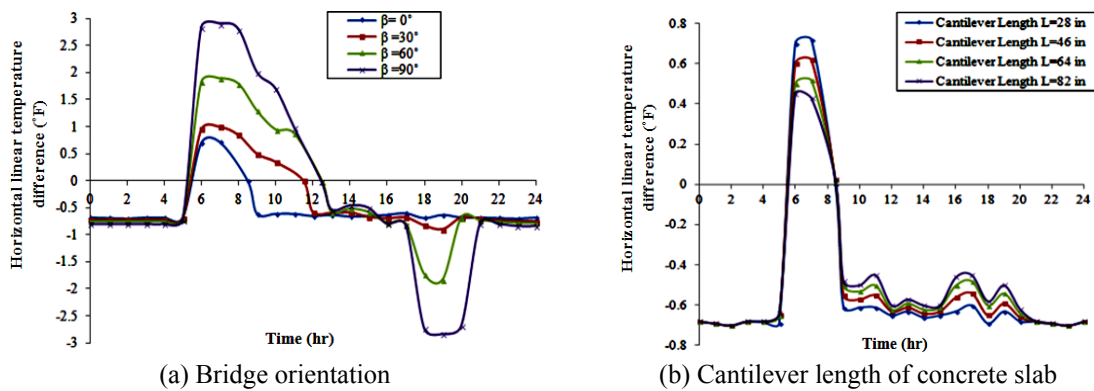


Fig. 8 Parametric investigations of the horizontal linear temperature difference

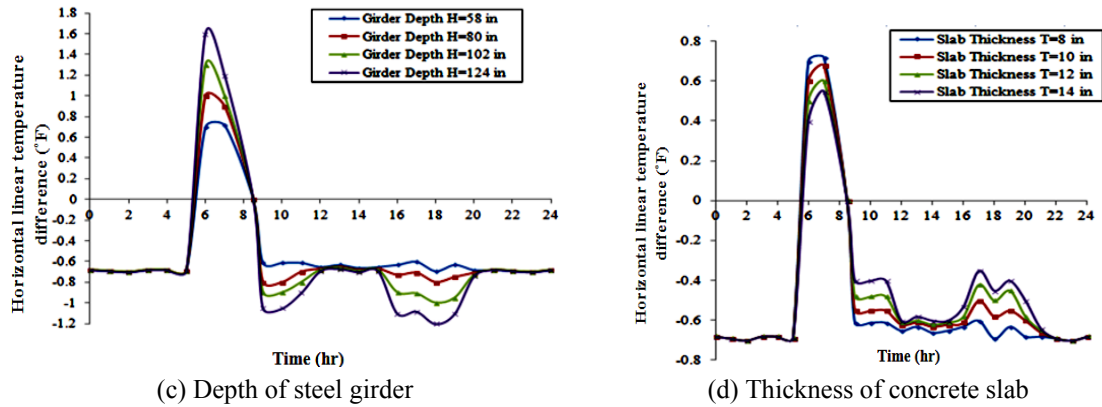


Fig. 8 Continued

due to the northern and southern faces of the bridge at $\beta = 90^\circ$ became more sunlit at the sunrise and the sunset hours than the other orientations, and thus the temperature in the steel plates were raised quicker.

From Figs. 8(b)-(d), it can be detected that the peak positive and negative of the horizontal linear temperature differences incident at around 07:00 a.m. and 06:00 p.m., respectively, when the section of CBGB lies under the effects following parameters: shorter cantilever length of the concrete slab, deeper steel web, and thinner concrete slab. In these figures, it can be also observed that the main differences between the horizontal thermal gradients occurred at the times when the steel webs of bridge exposed to direct sun rays.

6.3 The mean bridge temperature

As shown in Figs. 9(a)-(d), in general, the fashion of the mean bridge temperature curves was similar to the atmospheric temperature curve throughout the investigated day, which is shown in Fig. 4(a). This is due to a small thermal mass of the composition system of the bridge, and therefore the mean bridge temperature displayed a high correlation with the instantaneous atmospheric temperature.

The curves presented in Fig. 9(a)-(c) shows that the effect of orientation of the bridge's longitudinal axis, cantilever length of the concrete slab, and depth of steel girder on the mean bridge temperature were insignificant. Only very slight differences were determined at the sunrise and the sunset times when the faces of steel girder were open to sunlight. The behavior of these curves was also confirmed by the fact that the sun's rays became at the less level of intensity when the faces of steel plates were subjected to direct sun rays (often at the sunrise or the sunset time).

As seen from Fig. 9(d), the concrete slab thickness has a significant impact on the mean bridge temperature along 24 hours of the studied day than the other parametric investigations. As a matter of fact, the concrete slab receives rays of sun essentially through the top horizontal surface throughout the daytime. When the slab thickness increased from 8 to 14 inches, the proportion of the area of the top horizontal surface to the volume of the concrete slab becomes smaller. Thus, the mean bridge temperature dropped after about 11:00 a.m. to about 07:00 p.m. and rose except for those times due to the concrete is a weak conductor of heat.

However, for all ranges of the individual parameters, the highest and lowest values of the mean

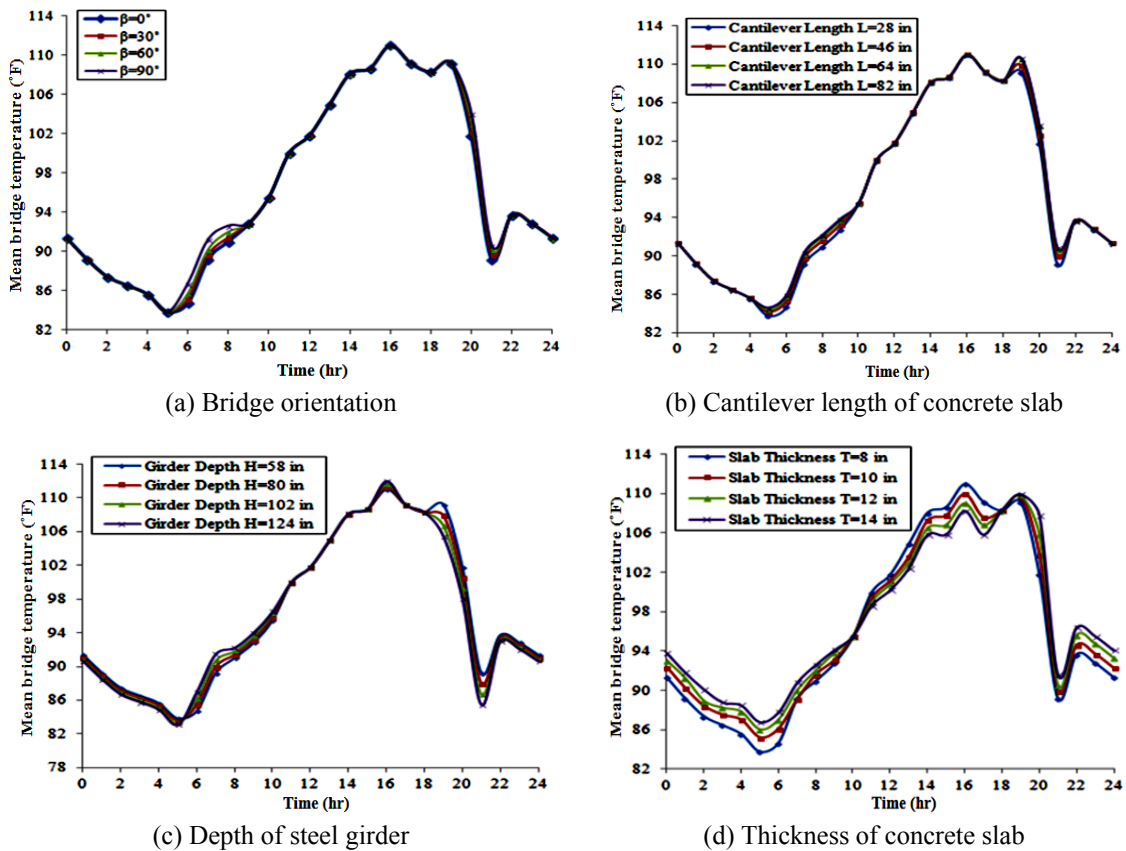


Fig. 9 Parametric investigations of the mean bridge temperature

bridge temperature occurred at approximately 05:00 a.m. and 04:00 p.m., respectively, as shown in Figs. 9(a)-(d).

6.4 The residual temperature of the concrete slab

As shown in Fig. 10(a), the absolute maximum value of the average concrete residual temperature took place at approximately 10:00 a.m. at $\beta = 90^\circ$, which was 9.54°F . As a result, the generated eigenstresses was about 0.22 ksi in the concrete slab, this can be attributed to the exposure of the side faces of the concrete slab at $\beta = 90^\circ$ to more sunlight at the sunrise and the sunset times than those for other orientations.

From Fig. 10(b), the absolute maximum value of the average concrete residual temperature was not sensitive to the cantilever length of concrete slab since it did not influence the shaded area of the concrete surface, and it achieved at about 12:10 p.m., which was 5.74°F . This residual temperature generated eigenstresses approximately 0.12 ksi in the concrete slab.

An increase in the web depth of the steel girder has an obvious impact on the average of concrete residual temperature over the day since the steel has a high relatively thermal conductivity, as shown in Fig. 10(c). It can be also noticed that the absolute maximum value of the average concrete residual temperature achieved at about 12:05 p.m., which was 5.81°F for all

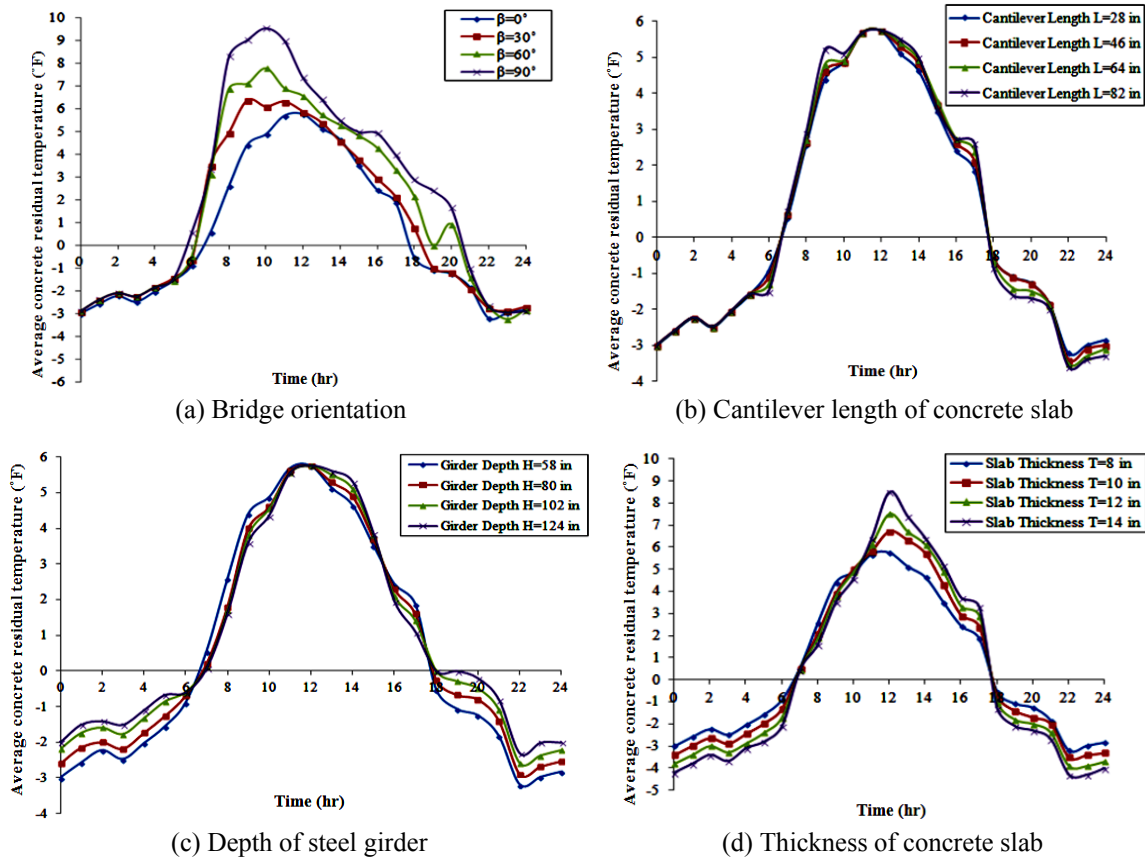


Fig. 10 Parametric investigations of the average residual temperature of the concrete slab

cases. The eigenstresses of about 0.13 ksi in the concrete slab relied on the occurrence of the absolute maximum value of the average concrete residual temperature.

As shown in Fig. 10(d) that the absolute maximum value of the average concrete residual temperature was 8.50°F, which occurred at the thickness of the concrete slab of 14 inches at about 12:15 p.m. This caused to the generation of eigenstresses in the concrete slab of approximately 0.19 ksi. This is owing to the behavior of temperature distribution across the concrete section since it became more nonlinear when the thickness of concrete slab increased.

6.5 The residual temperature of the steel girder

Fig. 11(a) shows that the largest absolute maximum value of the average steel residual temperature at around 09:00 a.m., which was 9.38°F, when the longitudinal axis of bridge oriented at $\beta = 90^\circ$, and hence, the developed eigenstresses was about 1.80 ksi in the steel section. This is because the CBGB model at $\beta = 90^\circ$ subjected to more sun rays than the other proposed orientations and the temperature in the steel web plates increases faster.

Fig. 11(b) illustrates the effect of the cantilever length of concrete slab on the average steel residual temperatures. The longest cantilever length caused the expansion of the shaded area on the steel faces. Therefore, the predicted values of the average steel residual temperature were

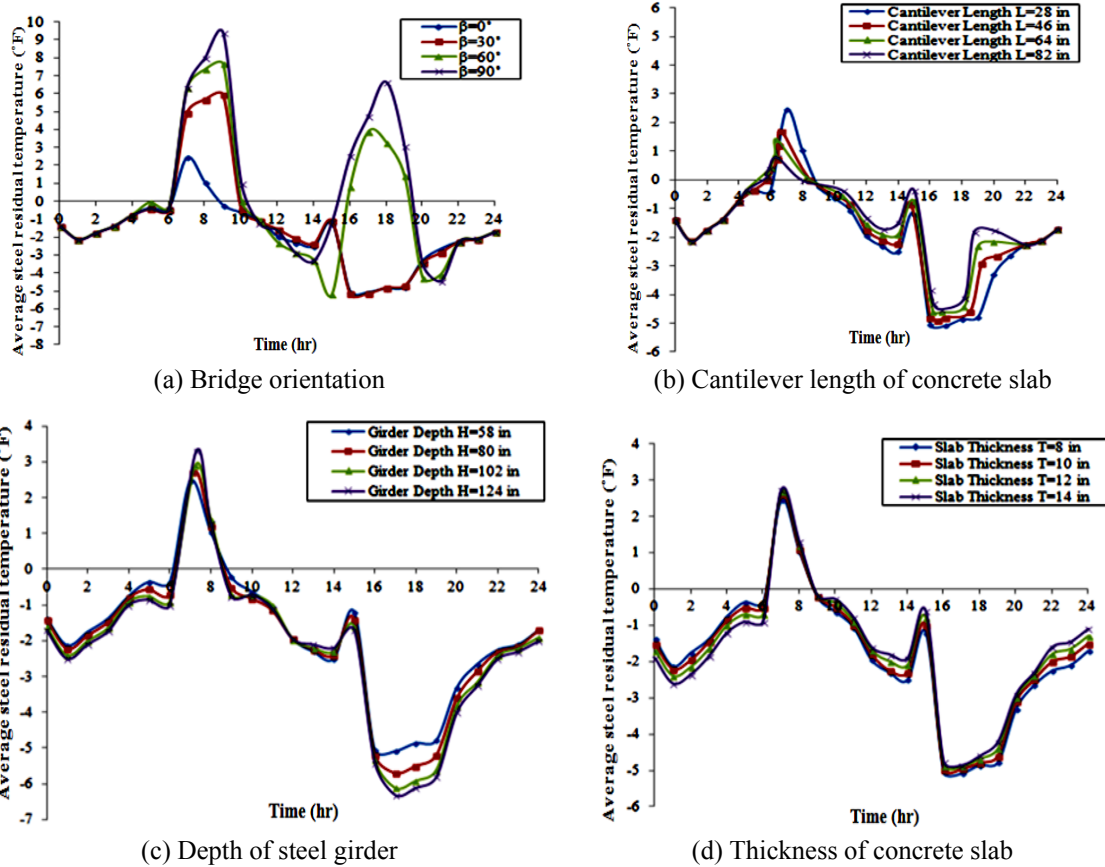


Fig. 11 Parametric investigations of the residual temperature of the steel girder

decreased. At about 05:00 p.m., the absolute maximum value of the average steel residual temperature was 5.10°F for the shortest cantilever concrete slab. This residual temperature caused to make the eigenstresses of about 0.93 ksi in steel section.

Fig. 11(c) demonstrates that the largest differences between the average steel residual temperature curves occurred from about 04:00 p.m. to approximately 07:00 p.m. This is due to the southern faces of the steel box were subjected to direct sunlight, as well as, the reflected radiations from the earth’s surface and the objects surrounding the bridge at this period. At the depth of steel web equal to 124 inches, the absolute maximum value recorded during the examined day of 6.30°F at approximately 05:00 p.m., and as a result, the induced eigenstresses was about 1.15 ksi in the steel section.

During the daily thermal cycle, there are relatively small differences between the average steel residual temperature curves when the thickness of concrete slab was increased, as depicted in Fig. 11(d). This is owing to the insulating properties of the concrete material, and as a result, the temperature distribution within a steel section was not much varied. At around 05:00 p.m., the absolute maximum value of the average steel residual temperature was achieved of 5.10°F for the thinnest concrete slab. Therefore, the developed eigenstresses in the steel section was about 0.93 ksi.

7. Conclusions

In this paper, a full-scale experimental CBGB segment and numerical thermal analyses were utilized to study the effects of geometrical parameters and orientation of the bridge on the time-dependent temperature distributions and eigenstresses.

The results from 3D FE analysis were compared with the experimental results, and a general good agreement was achieved, which reflects the ability of the current FE study to analyze the behavior of CBGB under the daily climatic variations. The COMSOL is a useful program to simulate the reciprocal irradiations heat transfer between the exposed surfaces of the bridge and ambient air simultaneously.

Based on the FE parametric investigations of the cross-section model; the following main conclusions about the thermal loading parameters can be summarized:

- The thickness of concrete slab had the highest individual influence among the four parametric investigations on the vertical linear temperature gradients. The maximum absolute difference of the vertical linear temperature occurred when the thickness of concrete slab decreased from 14 to 8 inches was more than 5.50°F at 03:00 p.m., while the maximum calculated absolute vertical linear temperature difference was 4.66°F at 08:00 a.m., as the orientation of the bridge's longitudinal axis changed from $\beta = 90^\circ$ to $\beta = 0^\circ$, while the maximum calculated absolute vertical linear temperature difference was about 4.20°F at 03:00 p.m., as the depth of steel girder decreased from 124 to 58 inches, and about 2.68°F at 04:00 p.m., as the cantilever length of the concrete slab increased from 28 to 82 inches.
- The orientation of bridge parameter has a greater influence on the horizontal linear temperature gradient than the other parameters. At 08:30 a.m., the maximum absolute difference between the horizontal linear temperature gradients occurred when the orientation of the longitudinal axis of the bridge changed from $\beta = 0^\circ$ to $\beta = 90^\circ$ and was more than 2.80°F. During the daily thermal cycle, the basic variances between horizontal linear temperature gradients needed to be assessed at the periods when the steel webs became sunlit. Other than that, the variances between gradients were relatively minimal. It should be noted that the higher ratios of the cantilever length of the concrete slab to girder depth of steel girder produced a smaller horizontal linear temperature difference.
- The hourly results of the mean bridge temperature curves under parametric investigations showed that those curves were similar to the behavior curve of atmospheric temperature to a great extent, where the minimum mean bridge temperature was achieved just before the sunrise, while the maximum mean bridge temperature was achieved in the late afternoon. The mean bridge temperatures were generally not sensitive to the bridge orientation, depth of steel girder, and cantilever length of concrete slab, but they were a very sensitive with the variation of the concrete slab thickness and the maximum absolute difference in the mean bridge temperature recorded at 5:00 p.m., which was 3.40°F when the concrete slab thickness reduced from 14 to 8 inches.
- When the orientation of bridge transformed from $\beta = 0^\circ$ to $\beta = 90^\circ$, the highest absolute difference happened in the average residual temperature of the concrete slab, which was approximately 5.71°F at 08:00 a.m., while the highest absolute difference happened in the average residual temperature of the steel girder was approximately 11.50°F at 06:00 p.m.

Based on the above results under the given weather actions, the ideal thermal loading parameter

curves are achieved under the following configurations of CBGB: E-W bridge orientation (at $\beta=0^\circ$), shorter steel girder webs, longer lengths of the concrete slab cantilever, in addition to thicker concrete slabs. These observations about the CBGB configurations may be used as reference information to evolve the guidelines of thermal design for such structures.

A closer look at the calculated hourly outcomes of the average residual temperatures illustrates that the design temperature distribution with a uniform differential between the concrete slab and the steel box girder is not suitable for capturing the thermo-structural behaviors of CBGBs. Furthermore, the current FE thermal analysis provides the opportunity to develop insights for future studies such as simulation the influences of the composite continuous box-girder bridge; and changing the thermal material properties of components on the sensitivity behavior of thermal loading parameters.

References

- Barber, E.S. (1957), "Calculation of maximum pavement temperatures from weather reports", Highway Research Board Bulletin, **168**, 1-8.
- Berwanger, C. (1970), "Thermal stresses in composite bridges", *Proceedings of ASCE Specialty Conference on Steel Structures, Engineering Extension Series*, University of Missouri-Columbia; Columbia, MO, USA, June.
- Berwanger, C. (1983), "Transient thermal behavior of composite bridges", *J. Struct. Eng., ASCE*, **109**(10), 2325-2339.
- Berwanger, C. and Symko, Y. (1975), "Thermal stresses in steel-concrete composite bridges", *Can. J. Civ. Eng.*, **2**(1), 66-84.
- Cao, Y., Yim, J., Zhao, Y. and Wang, M.L. (2011), "Temperature effects on cable stayed bridge using health monitoring system: a case study", *Struct. Ctr. Hlth.*, **10**(5), 523-537.
- Chang, J.B.J. and Robertson, I.N. (2003), "Computer modeling of the proposed Kealakaha stream bridge", Research Report; UHM/CEE/03-03, University of Hawaii System, HI, USA.
- Dilger, W.H., Ghali, A., Cheung, M.S. and Maes, M.A. (1983), "Temperature stresses in composite box girder bridges", *J. Struct. Eng., ASCE*, **109**(6), 1460-1478.
- Emanuel, J.H. and Hulsey, J.L. (1978), "Temperature distributions in composite bridges," *J. Struct. Div.*, **104**(1), 65-78.
- Fu, H.C., Ng, S.F. and Cheung, M.S. (1990), "Thermal behavior of composite bridges", *J. Struct. Eng.*, **116**(12), 3302-3323.
- Im, C.K. and Chang, S.P. (2004), "Estimating extreme thermal loads in composite bridge using long-term measured data", *Int. J. St. Structs.*, **4**(1), 25-31.
- Kehlbeck, F. (1975), "Effect of solar radiation on bridge structures", Hannover Technological University; Verlag-Press, Dusseldorf, DUS, Germany.
- Kennedy, J.B. and Soliman, M.H. (1987), "Temperature distribution in composite bridges", *J. Struct. Eng.*, **113**(3), 475-482.
- Kim, S.H., Cho, K.I., Won, J.-H. and Kim, J.H. (2009), "A study on thermal behavior of curved steel box girder bridges considering solar radiation", *Arch. Civ. Mech. Eng.*, **9**(3), 59-76.
- Larsson, O. and Karoumi, R. (2011), "Modelling of climatic thermal actions in hollow concrete box cross-sections", *Struct. Eng. Int.*, **21**(1), 74-79.
- Massicotte, B., Picard, A., Gaumont, Y. and Ouellet, C. (1994), "Strengthening of a long span prestressed segmental box girder bridge", *PCI J.*, **39**(3), 52-65.
- Moorthy, S. and Roeder, C.W. (1992), "Temperature-dependent bridge movements", *J. Struct. Eng.*, **118**(4), 1090-1105.
- Narouka, M., Hirai, I. and Yamaguti, T. (1957), "The measurement of the temperature of the interior of the reinforced concrete slab of the Shigita Bridge and presumption of thermal stress", *Proceedings of the*

- Symposium on the Stress Measurements for Bridge and Structures, Japan Society for the Promotion of Science*, Tokyo, Japan, December.
- Ni, Y.Q., Hua, X.G., Wong, K.Y. and Ko, J.M. (2007), "Assessment of bridge expansion joints using long-term displacement and temperature measurement", *J. Perform. Constr. Facil.*, **21**(2), 143-151.
- Stewart, C.F. (1967), "Long structures without expansion joints", Interim Report; California Department of Transportation, USA.
- Tong, M., Tham, L.G., Au, F.T.K. and Lee, P.K.K. (2001), "Numerical modelling for temperature distribution in steel bridges", *Comput. Struct.*, **79**(6), 583-593.
- Topkaya, C., Yura, J.A., Williamson, E.B. and Frank, K.H. (2005), "Composite Action during Construction of Steel Trapezoidal Box Girder Bridges", Research Report; FHWA/TX-07/0-1898-2, University of Texas, TX, USA.
- Troy, T.T. and Chai, H.Y. (1998), "Thermal effects on skewed highway bridges including bearing orientation", Research Report; Highway Research Center, Auburn University, AL, USA.
- William, G.W., Shoukry, S.N. and Riad, M.Y. (2005), "Thermal stresses in steel girder bridges with integral abutments", *Brdg. Structs.*, **1**(2), 103-119.
- Xu, Z.-D. and Wu, Z. (2007), "Simulation of the effect of temperature variation on damage detection in a long-span cable-stayed bridge", *Struct. Hlth. Monit.*, **6**(3), 177-189.
- Xu, Y.L., Chen, B., Ng, C.L., Wong, K.Y. and Chan, W.Y. (2010), "Monitoring temperature effect on a long suspension bridge", *Struct. Ctr. Hlth.*, **17**(6), 632-653.
- Xia, Y., Chen, B., Zhou, X.-Q. and Xu, Y.-L. (2013), "Field monitoring and numerical analysis of Tsing Ma Suspensions Bridge temperature behavior", *Struct. Ctr. Hlth.*, **20**(4), 560-575.
- Zuk, W. (1965), "Thermal behaviour of composite bridges-insulated and uninsulated", Highway Research Record 76; National Research Council, pp. 231-253.